

Photoreflectance line shape symmetry and quantum-well ground-state exciton energy in vertical-cavity surface-emitting laser structures

Sandip Ghosh, Thomas J. C. Hosea,^{a)} and Stephanie B. Constant
Department of Physics, University of Surrey, Guildford GU2 7XH, United Kingdom

(Received 21 December 2000; accepted for publication 28 March 2001)

We report photoreflectance studies on the coupling between the Fabry–Perot cavity mode (CM) and the quantum well (QW) ground-state excitonic feature in vertical-cavity surface-emitting laser structures. Changes in the symmetry of the CM-QW spectral feature occur when the angle of incidence of the probe beam is altered. Using detailed simulations, we explain how this is related to an unusual reversal of the roles of the Seraphin coefficients and QW dielectric function, in determining the line shape. Our study suggests a way to find the exciton energy, in situations where a distinct QW feature is not seen because of large broadening of the QW dielectric function combined with high reflectivity of Bragg mirrors and relatively narrow CM width. © 2001 American Institute of Physics. [DOI: 10.1063/1.1374233]

Interest in vertical-cavity surface-emitting lasers (VCSELs) has increased due to their superior characteristics compared to conventional edge emitters.¹ In VCSELs the relative energy positions of the single Fabry–Perot cavity mode (CM) and peak of the gain spectrum arising from the quantum well (QW) ground state excitonic transition in the active region, strongly influences the threshold current density, output power, and their temperature dependence.² While the CM energy (E_{CM}) is easy to find from a reflectance (R) spectrum, postgrowth nondestructive estimation of the QW exciton energy (E_{ex}) is difficult due to strong modification of all front surface spectra by the distributed Bragg reflectors (DBRs). Edge emission electroluminescence (EL),³ and photoluminescence (PL)⁴ have proved useful (but require cleaving). Nondestructive front surface photoreflectance (PR) works well if the top DBR reflectivity (R_T) is not too high ($<95\%$), and energy broadening (Γ_{ex}) of E_{ex} is small (<10 meV).⁵ If Γ_{ex} and CM broadening (Γ_{CM}) are small and comparable, and their energy positions are tuned to coincide by varying, e.g., position, temperature or pressure, then the resultant PR line shapes are complex. In such cases there is a resonance effect, i.e., the amplitude of the coupled CM-QW feature in PR increases significantly when E_{CM} and E_{ex} coincide, enabling estimation of E_{ex} .⁶ However, when R_T is high and Γ_{CM} is narrow, very little probe light (of energy on either side of E_{CM}) reaches the QW. In addition if Γ_{ex} is large (resulting in smaller amplitude of the exciton feature), then a separate exciton PR feature is not seen. Here, we show how, even in such cases, E_{ex} can be determined using PR, by studying the changing symmetry of the coupled CM-QW feature as a function of angle of incidence (θ_i) of the probe beam.

Two metalorganic-chemical-vapor-deposition grown representative samples were studied. VCSEL-1: infrared emitter with $Al_{0.15}Ga_{0.85}As/Al_{0.95}Ga_{0.05}As$ DBR [26 top pairs ($R_T=99\%$), 13 bottom], $Al_{0.2}Ga_{0.8}As$ cavity and four 12 nm $Ga_{0.84}In_{0.16}As/Ga_{0.08}As_{0.92}P$ QWs in the active region;

VCSEL-2: red emitter with $Al_{0.5}Ga_{0.5}As/Al_{0.98}Ga_{0.02}As$ DBR [8 top ($R_T=83\%$), 34 bottom], $(Al_{0.7}Ga_{0.3})_{0.52}In_{0.48}P$ cavity and four 6 nm $Ga_{0.42}In_{0.58}P/(Al_{0.5}Ga_{0.5})_{0.52}In_{0.48}P$ QWs. The PR setup had a 0.32 m monochromator dispersed probe beam, Ar^+ pump laser (8 mW), Si detector and phase-sensitive amplifier, locked into the phase of the scattered laser and/or associated PL.

Figure 1(a) shows the only feature (for different θ_i) seen in VCSEL-1, near the expected energy of E_{ex} . Its energy position is clearly determined by the CM since it follows the CM dip in R [Fig. 1(b)]. Here E_{ex} cannot be found by fitting the earlier line shape model,⁶ since the spectra do not show any of the complex structure appropriate to that model. Note, however, that the symmetry of the feature changes from a three-lobed symmetric structure ($\theta_i \approx 13^\circ$) to twin-lobed antisymmetric (25°) and then back to three-lobed symmetric, but of opposite phase (40°).

This, we suggest, arises from a coupling between CM and QW ground state exciton feature. In general, the PR line shape can be expressed as $\Delta R/R = \alpha \Delta \epsilon_1 + \beta \Delta \epsilon_2$, where $\alpha = (1/R)(\partial R/\partial \epsilon_1)$, $\beta = (1/R)(\partial R/\partial \epsilon_2)$ are the Seraphin coefficients, and $\Delta \epsilon_{1,2}$ are the modulation induced changes in the

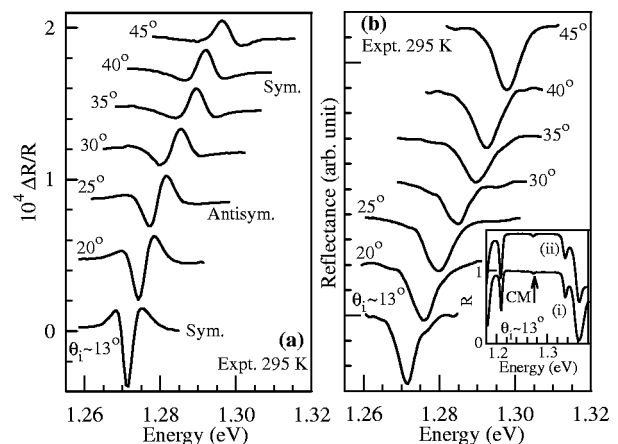


FIG. 1. (a) CM-QW feature in PR, and (b) the CM feature in R of VCSEL-1, for different θ_i . Inset: the full high-reflectance stop band [experiment (i) and simulation (ii)] for $\theta_i \approx 13^\circ$.

^{a)}Electronic mail: j.hosea@surrey.ac.uk

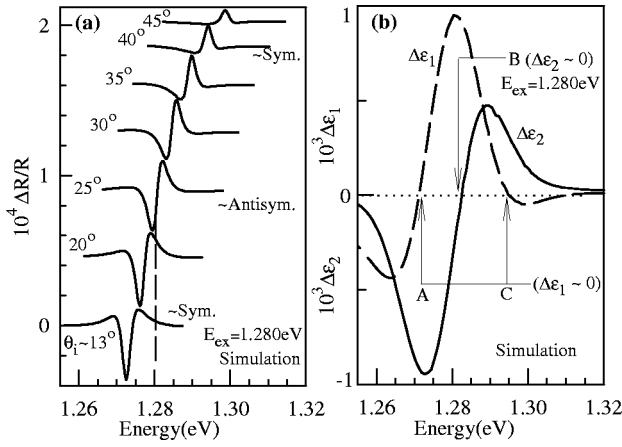


FIG. 2. (a) Simulated CM-QW feature in PR of VCSEL-1; (b) energy dependence of QCSE-induced $\Delta\epsilon_1$ and $\Delta\epsilon_2$ for VCSEL-1.

dielectric function ϵ .⁷ To verify our hypothesis we performed simulations as follows. The chopped pump beam reduces the built-in electric field. This modulates the exciton ϵ , via the quantum confined Stark effect (QCSE),⁸ the dominant effect being a shift ΔE_{ex} in E_{ex} .^{9,10} We considered an ϵ of the form¹¹

$$\epsilon(E) = \epsilon_{\infty} + (fe^2\hbar^2/\mu\epsilon_0L_z)[1/(E_{ex}^2 - E^2 - i\gamma_{ex}E)], \quad (1)$$

where L_z , f ($2 \times 10^{15} \text{ m}^{-2}$), μ ($0.06 m_0$), and γ_{ex} (6 meV) are the well width, exciton oscillator strength, reduced mass and homogenous broadening, respectively.^{11,12} Other symbols have their usual meaning. To account for the inhomogeneous broadening due to fluctuations in L_z or composition, a normalized Gaussian distribution of E_{ex} values (mean 1.28 eV) was used for averaging ϵ . Interband absorption at energies above the exciton binding energy was also included. The R of the complete VCSEL structure was calculated using transfer matrices,¹³ with refractive indices from Ref. 14. ΔR was found from the difference between R calculated with $E_{ex} + \Delta E_{ex}$ and E_{ex} in Eq. (1). This automatically incorporates α , β , and $\Delta\epsilon_{1,2}$ in the calculations. From matching the simulation with experiment, ΔE_{ex} and the total exciton broadening Γ_{ex} obtained were $\approx 60 \mu\text{eV}$ and $\approx 18 \text{ meV}$, respectively. Thus $\Gamma_{ex} \gg \Gamma_{CM}$ (5 meV) which is crucial here.

Figure 2(a) shows the simulated PR spectra of VCSEL-1, which reproduce well the experimental symmetry variations of the CM-QW feature. Figure 2(b) shows the calculated energy dependence of the QCSE-induced $\Delta\epsilon_{1,2}$. If we assume $\Delta\epsilon_1$ is constant and $\Delta\epsilon_2 = 0$, the simulated PR line shape is in general antisymmetric, while a symmetric one results when $\Delta\epsilon_1 = 0$ and $\Delta\epsilon_2$ constant [see Figs. 3(a) and 3(b)]. Changing the signs of $\Delta\epsilon_{1,2}$ phase shifts these line shapes by π . One can understand all of this physically as follows. A change in ϵ_1 affects the optical thickness of the cavity region, which modulates the CM energy in R [see schematic inset of Fig. 3(a)]. The difference between these two R spectra yields the antisymmetric ΔR . On the other hand, a change in ϵ_2 alters the cavity absorption, which modulates the depth of the CM [inset of Fig. 3(b)], the difference giving a symmetric ΔR . If both $\Delta\epsilon_{1,2}$ are nonzero, the line shape is asymmetric. Returning to Fig. 2(b), at an energy lower than E_{ex} (point A), $\Delta\epsilon_1 \approx 0$ and $\Delta\epsilon_2 \approx$ negative constant. At point B, around $E \approx E_{ex}$, $\Delta\epsilon_1$

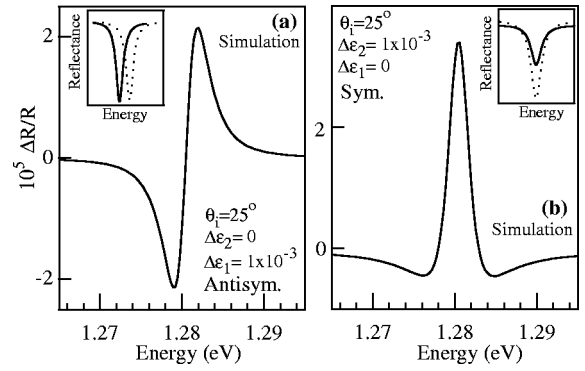


FIG. 3. Influence of (a) $\Delta\epsilon_1$ and (b) $\Delta\epsilon_2$ changes on the symmetry of the CM-QW feature in PR of VCSEL-1 (= Seraphin coefficients $\times 10^{-3}$). Insets: schematic of corresponding changed (line) and original (dotted) CM feature in R .

\approx positive constant and $\Delta\epsilon_2 \approx 0$. At point C, $\Delta\epsilon_1 \approx 0$ and $\Delta\epsilon_2 \approx$ positive constant. Thus, as E_{CM} is increased by θ_i tuning, the CM-QW PR feature is: first dominated by a symmetric shape when E_{CM} is at A; antisymmetric at B, and then symmetric again at C (but of opposite phase to that at A). This shows that $E_{ex} \approx E_{CM}$ at that θ_i where the CM-QW feature is approximately antisymmetric, occurring between two approximately symmetric features of opposite phase. At higher energies the line shape symmetry is likely to be influenced by contributions to $\Delta\epsilon_{1,2}$ from higher order transitions. The antisymmetric line shape occurs for VCSEL-1 in Fig. 1 at $\theta_i \approx 25^\circ$, yielding $E_{ex} \approx 1.281 \text{ eV}$, close to 1.28 eV used in simulations. This was further confirmed by edge emission EL³ (1.280 eV).

The present phenomenon is different from other known cases of phase rotation in PR.¹⁵ Normally the PR line shape is determined mainly by $\Delta\epsilon_{1,2}$, because they vary much more rapidly with energy than α , β . The latter are treated as constants, determining only the relative contributions of $\Delta\epsilon_{1,2}$ to the spectrum, and thus its phase. Any change in α , β , e.g., due to interference effects, shifts the PR phase. The line shapes in Figs. 3(a) and 3(b) actually also equal the α , β (divided by 10^3) of VCSEL-1 in the vicinity of the CM. Here, α , β vary much more rapidly with energy than $\Delta\epsilon_{1,2}$ (because $\Gamma_{ex} \gg \Gamma_{CM}$) and therefore it is α , β which determine the PR line shape. The changes in symmetry and phase arise from the relative contributions of α and β , as determined by the magnitude and sign of $\Delta\epsilon_{1,2}$. In other words, the roles of $\Delta\epsilon_{1,2}$ and α , β are reversed compared to the conventional situation.

As additional evidence we present results on VCSEL-2, which has fewer top DBR pairs, therefore allowing observation of a QW exciton feature, in the $\theta_i \approx 13^\circ$ PR spectrum [Fig. 4(a)]. Here too Γ_{ex} (18 meV) $\gg \Gamma_{CM}$ (8 meV), and similar symmetry variations occur as the CM is tuned across E_{ex} (1.908 eV in simulations, 1.905 eV in edge EL). The simulations [Fig. 4(b)] reproduce this effect, confirming our argument. We can also reproduce the more complex line shapes and resonance effect seen when the QW and CM widths are small and comparable.⁶ Then, however, there need not be a simple symmetry to the line shape near resonance, since the energy dependence of α , β , and $\Delta\epsilon_{1,2}$ all come into play. In general, the relative amplitudes of α and β depend on the VCSEL structure and also the relative positions of E_{CM} and

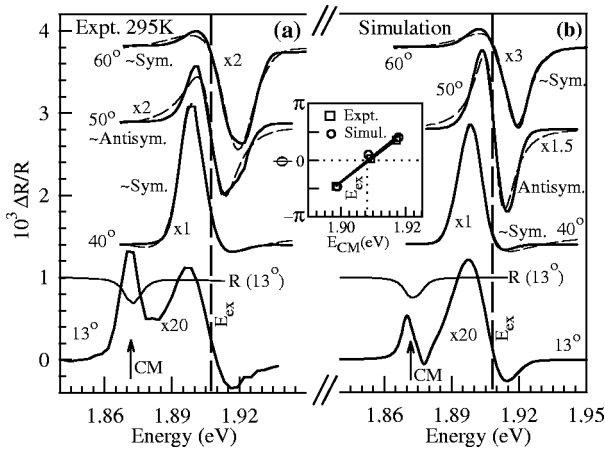


FIG. 4. (a) Experimental and (b) simulated coupled CM-QW feature in PR of VCSEL-2. At $\theta_i \approx 13^\circ$ there are distinct features from the QW, and CM (also seen in R). Inset: plot of ϕ vs E_{CM} , obtained from fitting Eq. (2) (with $m=2$) to both experimental and simulated spectra (fits shown by dashed lines), for $\theta_i \geq 40^\circ$.

E_{ex} (since ϵ_2 varies strongly near E_{ex}). The simulations show that if $\beta \gg \alpha$ (with $\Gamma_{ex} \gg \Gamma_{CM}$) an antisymmetric line shape may still occur when $E_{CM} \approx E_{ex}$, but will be weaker than the symmetric line shapes occurring when E_{CM} is on either side of E_{ex} (i.e., an amplitude antiresonance). In fact, VCSEL-2 represents such a case [see Fig. 4(a)] since our calculations show that the amplitude of β near E_{ex} is about five times that of α . Thus, the symmetry aspect (rather than amplitude) continues to be the more reliable indicator of when $E_{CM} \approx E_{ex}$.

Thus, for VCSELs in which $\Gamma_{ex} \gg \Gamma_{CM}$, the CM-QW line shape is essentially a linear combination of the Seraphin coefficients, such as those in Fig. 3. Several approximate empirical descriptions of its symmetry are possible; here we choose a conventional PR model:⁷

$$L(E) = \Re e [a \Gamma^m e^{i[\phi + (m-3)\pi/2]} / (E - E' + i\Gamma)^m], \quad (2)$$

only, now Γ and a represent the broadening and amplitude of the CM-QW feature, respectively, and $E' \approx E_{CM}$. The exponent m can be chosen to be 2 or 3. The parameter of interest here is the (m independent) phase ϕ which is a measure of relative magnitudes of α and β and their contribution to the CM-QW feature, and thus its symmetry, $\phi=0$ or π giving antisymmetry. Thus, according to our argument, a plot of ϕ vs E_{CM} [obtained by fitting Eq. (2) to the CM-QW feature] should yield E_{ex} from the value of E_{CM} at which $\phi=0$ or π . This is true for VCSEL-2 (Fig. 4, inset). Thus E_{ex} can be

found by measurements at a few θ_i spanning the symmetry change, none of which need correspond to the case of $E_{CM} \approx E_{ex}$, since interpolation can be used. Tuning θ_i from 0° can only blueshift E_{CM} . However, all VCSEL designs have $E_{ex} > E_{CM}$ for $\theta_i = 0^\circ$ at 295 K, so that during operation, heating-induced redshift of the gain peak aligns it with the CM.² Therefore, θ_i tuning can in principle always be used to find E_{ex} , unless growth is far from the specification. Note that our analysis does not involve an exciton–polariton since no explicit exciton–photon interaction term was involved. Our case derives from the linear-dispersion-model description of the phenomenon of Rabi splitting in microcavities.¹⁶

The authors thank T. E. Sale, S. J. Sweeney, A. Onischenko, and A. R. Adams for useful discussions.

- ¹K. Iga, F. Koyama, and S. Kinoshita, *IEEE J. Quantum Electron.* **QE-24**, 1845 (1988).
- ²T. E. Sale, *Vertical Cavity Surface Emitting Lasers* (Research Studies, Taunton, 1995), and references therein.
- ³S. Ghosh, S. Constant, T. J. C. Hosea, and T. E. Sale, *J. Appl. Phys.* **88**, 1432 (2000).
- ⁴S. Gramlich, J. Sebastian, M. Weyers, and R. Hey, *Phys. Status Solidi A* **152**, 293 (1995).
- ⁵P. D. Berger, C. Bru, T. Benyattou, G. Guillot, A. Chenevas-Paule, L. Couturier, and P. Grosse, *Appl. Phys. Lett.* **68**, 4 (1996); Y. S. Huang, L. Malikova, F. H. Pollak, H. Shen, J. Pamulapati, and P. Newman, *ibid.* **77**, 37 (2000).
- ⁶P. J. Klar, G. Rowland, P. J. S. Thomas, A. Onischenko, T. E. Sale, T. J. C. Hosea, and R. Grey, *Phys. Rev. B* **59**, 2894 (1999); P. M. A. Vicente, P. J. S. Thomas, D. Lancefield, T. E. Sale, T. J. C. Hosea, A. R. Adams, P. J. Klar, and A. Raymond, *Phys. Status Solidi B* **211**, 255 (1999).
- ⁷D. E. Aspnes, in *Handbook of Semiconductors*, edited by M. Balkanski (North-Holland, New York, 1980), Vol. 2; D. E. Aspnes, *Surf. Sci.* **37**, 418 (1973).
- ⁸D. A. B. Miller, D. S. Chemla, T. C. Damen, A. C. Gossard, W. Wiegmann, T. H. Wood, and C. A. Burrus, *Phys. Rev. B* **32**, 1043 (1985).
- ⁹P. C. Klipstein and N. Apsley, *J. Phys. C* **19**, 6461 (1986).
- ¹⁰W. M. Theis, G. D. Sanders, C. E. Leak, K. K. Bajaj, and H. Morkoç, *Phys. Rev. B* **37**, 3042 (1988).
- ¹¹R. Houdre, R. P. Stanley, U. Oesterle, M. Ilegems, and C. Weisbuch, *Phys. Rev. B* **49**, 16 761 (1994).
- ¹²G. Bastard, *Wavemechanics Applied to Semiconductor Heterostructures* (Halsted, New York, 1988).
- ¹³E. Hecht, *Optics* (Addison-Wesley, Reading, MA, 1998).
- ¹⁴*Handbook of Optical Constants of Solids*, edited by E. D. Palik (Academic, New York, 1985).
- ¹⁵A. J. Shields and P. C. Klipstein, *Phys. Rev. B* **43**, 9118 (1991); R. A. Batchelor and A. Hammet, *J. Appl. Phys.* **71**, 2414 (1992); T. J. C. Hosea, P. J. Huges, and B. L. Wiess, *ibid.* **77**, 2672 (1995); R. T. Carline, T. J. C. Hosea, and D. J. Hall, *J. Appl. Phys.* **78**, 4285 (1995).
- ¹⁶Y. Zhu, D. J. Gauthier, S. E. Morin, Q. Wu, H. J. Carmichael, and T. W. Mossberg, *Phys. Rev. Lett.* **64**, 2499 (1990).